

# Biased Galaxy Formation And Measurements Of $\beta$

Andreas A. Berlind <sup>1</sup>, Vijay K. Narayanan <sup>2</sup>, and David H. Weinberg <sup>1</sup>

## ABSTRACT

Measurements of the cosmological density parameter  $\Omega_m$  using techniques that exploit the gravity-induced motions of galaxies constrain, in linear perturbation theory, the degenerate parameter combination  $\beta = \Omega_m^{0.6}/b$ , where the linear bias parameter  $b$  is the ratio of the fluctuation amplitudes of the galaxy and mass distributions. However, the relation between the galaxy and mass density fields depends on the complex physics of galaxy formation, and it can in general be non-linear, stochastic, and perhaps non-local. The one-parameter linear bias model is almost certainly oversimplified, which leads to the obvious question: What is the quantity  $\beta$  that is actually measured by different techniques? To address this question, we estimate  $\beta$  from galaxy distributions that are constructed by applying a variety of locally biased galaxy formation models to cosmological N-body simulations. We compare the values of  $\beta$  estimated using three different techniques: a density-density comparison similar to the POTENT analysis, a velocity-velocity comparison similar to the VELMOD analysis, and an anisotropy analysis of the redshift-space power spectrum. In most cases, we find that  $\beta$  estimated using all three methods is similar to the asymptotic value of  $\Omega_m^{0.6}/b_\sigma(R)$  at large  $R$ , where  $b_\sigma(R)$  is the ratio of rms galaxy fluctuations to rms mass fluctuations on scale  $R$ . Thus, something close to the conventional interpretation of  $\beta$  continues to hold even for complex bias models. Moreover, we find that  $\beta$  estimates made using these three methods should, in principle, agree with each other. It is thus unlikely that non-linear or scale-dependent bias is responsible for the discrepancies that exist among current measurements of  $\beta$  from different techniques.

*Subject headings:* cosmology: theory, galaxies: distances and redshifts, methods: numerical

---

<sup>1</sup>Department of Astronomy, The Ohio State University, Columbus, OH 43210; Email: aberlind,dhw@astronomy.ohio-state.edu

<sup>2</sup>Department of Astrophysical Sciences, Princeton University, Princeton, NJ 08544-1001; Email: vijay@astro.princeton.edu

## 1. Introduction

In cosmological linear perturbation theory, there is a simple relation between the peculiar velocity and the mass density fields,

$$\mathbf{v}(\mathbf{x}) = \frac{f(\Omega_m)}{4\pi} \int \delta_m(\mathbf{x}') \frac{(\mathbf{x}' - \mathbf{x})}{|\mathbf{x}' - \mathbf{x}|^3} d^3x' , \quad (1)$$

where  $\delta_m(\mathbf{x}) \equiv \rho(\mathbf{x})/\bar{\rho} - 1$  is the mass density contrast,  $f(\Omega_m) \approx \Omega_m^{0.6}$ , and  $\Omega_m$  is the ratio of the average mass density of the universe to the critical density (Peebles 1980). The differential form of this relation is

$$\vec{\nabla} \cdot \mathbf{v}(\mathbf{x}) = -f(\Omega_m)\delta_m(\mathbf{x}) . \quad (2)$$

These relations suggest that if we map the mass density and velocity fields, a comparison of the two will yield a measurement of  $\Omega_m$ . Unfortunately, we cannot observe the mass distribution directly. We can only detect luminous matter, of which galaxies are the basic unit. The relation between the galaxy and mass distributions, usually referred to as “bias”, depends on the details of the galaxy formation process. A complete theory of galaxy formation should predict what environments galaxies form in and how they are distributed in space with respect to the mass. However, while galaxy formation is one of the most actively pursued fields of theoretical cosmology, our current understanding of it is far from perfect. The relation between galaxies and mass is often parameterized by the linear bias model  $\delta_g = b\delta_m$ , where  $\delta_g$  is the galaxy density contrast and  $b$  is the linear bias factor. Equation (2) then becomes

$$\vec{\nabla} \cdot \mathbf{v}(\mathbf{x}) = -\beta\delta_g(\mathbf{x}) , \quad (3)$$

where  $\beta = f(\Omega_m)/b$ .

Methods that use equation (3), or some form of it, to infer the cosmic mass density can only directly measure  $\beta$ , a degenerate combination of  $\Omega_m$  and  $b$ . In practice,  $\beta$  is usually estimated from a comparison between the galaxy density field, inferred from galaxy redshift maps, and galaxy peculiar velocities, which require distance measurements to individual galaxies. This estimate is made either through a density-density comparison, where the mass density field is predicted from the smoothed peculiar velocity field and is then compared to the observed galaxy density field, or through a velocity-velocity comparison, where galaxy peculiar velocities are predicted from the galaxy density field and are then compared individually to observed galaxy peculiar velocities. Alternatively,  $\beta$  can be measured solely from galaxy redshift maps by analyzing the anisotropy of galaxy clustering produced by redshift-space distortions, using either the power spectrum or correlation function in redshift space. Based on these three main approaches, there are many techniques that have been developed and used to estimate  $\beta$  (see Strauss & Willick 1995 for a review of these techniques).

Since the bias relation depends on the complex process of galaxy formation, it is probably more complicated than the one-parameter linear bias model. It can, in general, be non-linear, stochastic, and possibly non-local (Dekel & Lahav 1999). Therefore, it is not obvious exactly what information a measurement of  $\beta$  contains. Moreover, it is not clear whether the different techniques for estimating  $\beta$  are measuring the same quantity. The primary purpose of this paper

is to examine these issues and determine what can be learned about bias from measurements of  $\beta$ . We create simulated galaxy distributions with various non-trivial bias prescriptions and use them to measure  $\beta$  with different existing techniques. The general approach is similar to the one we followed in Narayanan, Berlind & Weinberg (2000) (hereafter NBW), where we investigated the sensitivity of large-scale structure statistics to bias.

An additional motivation for this study is that there are large discrepancies in current  $\beta$  measurements made with different methods. For example, analyses of the IRAS 1.2-Jy galaxy redshift survey (Fisher et al. 1995) have yielded  $\beta_{IRAS} = 0.89 \pm 0.12$  by the density-density approach (Sigad et al. 1998),  $\beta_{IRAS} = 0.50 \pm 0.04$  by the velocity-velocity approach (Willick & Strauss 1998), and  $\beta_{IRAS} = 0.52 \pm 0.13$  by the redshift-space distortion approach (Cole, Fisher & Weinberg 1995). Table 1 summarizes current  $\beta$  estimates for IRAS-selected samples of galaxies made using different techniques. The estimates of  $\beta$  span the range 0.4 – 1.0, and the most extreme measurements differ from each other at the  $\sim 4\sigma$  level. Some authors have suggested that these discrepancies could be caused by complexity in the bias relation affecting different methods in different ways (Willick et al. 1997; Sigad et al. 1998; Dekel & Lahav 1999). For example, each technique effectively probes the bias on a different physical scale, so it is plausible that a scale-dependent bias relation could cause such discrepancies. In this paper we examine whether the variation in measured values of  $\beta$  can be naturally explained by complexity of bias.

We employ a variety of simple, non-linear, local bias prescriptions to create galaxy distributions from the outputs of N-body simulations. We then measure  $\beta$  using somewhat idealized versions of three different methods: a density-density comparison, a velocity-velocity comparison, and an analysis of the anisotropy of the redshift-space power spectrum. We assume that galaxy positions and peculiar velocities are known perfectly, and we therefore do not attempt to model the random and systematic errors that exist in real data. We are thus able to isolate the effects of different types of local biasing on measurements of  $\beta$  without worrying about how these measurements will be affected by observational errors. The systematic errors that exist in real observations are, of course, very important, but they are best dealt with in the context of specific data sets. We compare our  $\beta$  measurements to two well-defined functions. The first is  $\beta_\sigma(R) = \Omega_m^{0.6}/b_\sigma(R)$ . Here,  $b_\sigma(R)$  is the bias function defined as  $b_\sigma(R) = \sigma_g(R)/\sigma_m(R)$ , where  $\sigma_g(R)$  and  $\sigma_m(R)$  are the rms fluctuations of the galaxy and mass density fields, smoothed with a top-hat filter of radius  $R$ . The second function is  $\beta_P(k) = f(\Omega_m)/b_P(k)$ , where  $b_P(k)$  is the bias function in Fourier space, defined as  $b_P(k) = \sqrt{P_g(k)/P_m(k)}$ , where  $P_g(k)$  and  $P_m(k)$  are the power spectra of the galaxy and mass distributions. In NBW we demonstrated that, for local bias models,  $b_\sigma(R)$  and  $b_P(k)$  become scale-independent at large scales. We denote the asymptotic large-scale values of  $\beta_\sigma(R)$  and  $\beta_P(k)$  as  $\beta_\sigma$  and  $\beta_P$ , respectively.

## 2. Models

We have carried out N-body simulations of three different cosmological models, all based on inflation and cold dark matter (CDM). The first is an  $\Omega_m = 1$ ,  $h = 0.5$  model ( $h \equiv H_0/100 \text{ km s}^{-1} \text{ Mpc}^{-1}$ ), with a tilted power spectrum of density fluctuations designed to satisfy both COBE and cluster normalization constraints. The cluster constraint requires

$\sigma_{8m}\Omega_m^{0.6} \approx 0.55$  (White, Efstathiou & Frenk 1993), where  $\sigma_{8m}$  is the rms amplitude of linear mass density fluctuations in top-hat spheres of radius  $8h^{-1}\text{Mpc}$ . Matching the COBE-DMR constraint and  $\sigma_{8m} = 0.55$  with  $h = 0.5$  requires an inflationary spectral index  $n = 0.803$  if one incorporates the standard inflationary prediction for gravitational wave contributions to the COBE anisotropies (see Cole et al. 1997 and references therein). The other two models have  $\Omega_m = 0.2$  and  $0.4$ , with a power spectrum shape parameter  $\Gamma = 0.25$  (in the parameterization of Efstathiou, Bond & White 1992) and a cluster-normalized fluctuation amplitude  $\sigma_{8m} = 0.55\Omega_m^{-0.6}$ . These two models are open models with no cosmological constant ( $\Omega_\Lambda = 0$ ). Since  $\Omega_\Lambda$  has a negligible effect on peculiar velocities at fixed  $\Omega_m$ , our results for the two open models should also hold for flat- $\Omega_\Lambda$  cosmologies having the same values of  $\Omega_m$  and the same matter power spectrum. All simulations were run with a particle-mesh (PM) N-body code written by C. Park, which is described and tested by Park (1990). Each simulation uses a  $400^3$  force mesh to follow the gravitational evolution of  $200^3$  particles in a periodic cube  $400h^{-1}\text{Mpc}$  on a side, starting at  $z = 23$  and advancing to  $z = 0$  in 46 steps of equal expansion factor  $a$ . We have run four independent realizations of each of the above cosmological models, and all of the results shown in this paper have been averaged over these four realizations.

The bias between galaxies and mass should ultimately be a prediction of a theory of galaxy formation. There are currently three theoretical approaches to predicting how galaxies are distributed in space with respect to the mass. Semi-analytic models of galaxy formation identify virialized dark matter halos in moderate resolution N-body simulations and then populate them with galaxies using analytic prescriptions (e.g., Kauffmann et al. 1999; Benson et al. 2000); high resolution N-body simulations resolve individual galaxy-sized dark matter halos within larger halos (e.g., Kravtsov & Klypin 1999; Colín et al. 1999; Moore et al. 1999); hydrodynamic simulations follow the evolution of both dark matter and baryons, including the effects of gas cooling, star formation, and feedback, and identify galaxies based on the location of cold baryonic lumps (e.g., Cen & Ostriker 1992; Katz, Hernquist & Weinberg 1992; Katz, Weinberg & Hernquist 1996; Blanton et al. 1999; Pearce et al. 1999). All three approaches have made much progress in the last few years, but we are still far from a complete and compelling theory of galaxy formation, and even the most ambitious applications of these techniques have explored only a small selection of cosmological models and relatively small simulation volumes. Rather than adopt a specific, detailed theory of bias, we employ a simple approach to modeling the “generic” effects of bias on large-scale structure measurements. We apply plausible biasing schemes to select galaxy particles from the mass distributions and check which measurements of  $\beta$  are sensitive to the details of the biasing scheme and which are robust, extending the approach used by NBW (see also Mann, Peacock & Heavens 1998).

We create galaxy distributions by applying various local biasing prescriptions to the mass distributions. In these bias prescriptions, the probability of a given mass particle being selected as a galaxy depends on the properties (density, geometry, or velocity dispersion) of the mass distribution, averaged in top-hat spheres of radius  $4h^{-1}\text{Mpc}$ , centered on that particle. These prescriptions are also used and described in more detail by NBW and Narayanan et al. (1999). In brief, the bias prescriptions are:

- (1) Semi-analytic: An empirical bias prescription derived by Narayanan et al. (1999) which characterizes the relation between the galaxy and mass density fields in the semi-analytic galaxy

formation models of Benson et al. (2000).

(2) Sqrt-Exp (Square-root Exponential): A bias prescription in which  $(1 + \delta_g) \propto \sqrt{(1 + \delta_m)e^{\alpha(1 + \delta_m)}}$ . Here,  $(1 + \delta_g)$  and  $(1 + \delta_m)$  are the galaxy and mass overdensities, respectively. This prescription is intended to be monotonic (for  $\alpha > 0$ ) and non-linear, but it can be tuned to allow galaxies to be either biased or anti-biased with respect to the mass, and it yields a non-trivial bias relation even when  $b_\sigma = 1$ .

(3) Power-law: A bias prescription in which  $(1 + \delta_g) \propto (1 + \delta_m)^\alpha$ . This is similar to the bias relation suggested by Cen & Ostriker (1993), based on hydrodynamic simulations.

(4) Threshold: A bias prescription in which galaxies do not form below some mass density threshold, and they form with equal efficiency at densities above that threshold.

(5) Sigma: A bias prescription in which galaxies are selected with equal probability from mass particles that have a velocity dispersion  $\sigma_v$  greater than some threshold value.

(6) Sheet: A bias prescription that selects galaxies in regions where the mass distribution is planar. We compute the eigenvalues ( $\lambda_3 > \lambda_2 > \lambda_1$ ) of the moment of inertia tensor in spheres of radius  $4h^{-1}\text{Mpc}$  around each mass particle and select galaxies to be those mass particles that have the highest ratio of  $\lambda_3/\lambda_1$ .

(7) High- $z$ : A bias prescription identical to the Power-law bias, except galaxies are selected based on the mass distribution at redshift  $z = 3$ . This prescription is intended to produce a biasing relation that is stochastic on the  $4h^{-1}\text{Mpc}$  scale at  $z = 0$ , though still biased in the mean.

Each of the bias models contains one tunable parameter that is adjusted so that the resulting galaxy distribution has an rms fluctuation, in top-hat spheres of radius  $12h^{-1}\text{Mpc}$ , of  $\sigma_{12} \approx 0.7$ . The values of  $b_\sigma(12)$  for the galaxy distributions are 1.7, 1.0, and 0.67 for  $\Omega_m = 1.0, 0.4,$  and 0.2, respectively. In all the analyses in this paper, we form the mass and galaxy density fields by cloud-in-cell (CIC) binning the particle distributions onto a  $200^3$  grid. We create a volume-weighted, smoothed velocity field from the discrete galaxy peculiar velocities using the method of Babul et al. (1994). Specifically, we first form the momentum field by CIC-binning the momentum of every galaxy onto a  $200^3$  grid. We smooth this momentum field with a Gaussian filter of radius  $R_1 = R_s/2$  and divide it by a similarly smoothed density field to form a mass-weighted smoothed velocity field. We then smooth this velocity field with another Gaussian filter of radius  $R_2 = (R_s^2 - R_1^2)^{1/2}$ , so that the effective smoothing radius is  $R_s$ . Because the second smoothing dominates over the first, the final velocity field is volume-weighted rather than mass-weighted.

### 3. Density-Density Comparison

Density-density comparisons make direct use of equation (3) to measure  $\beta$ . The whole process, however, involves many steps. Radial peculiar velocities must first be computed for a sample of galaxies that have both redshift and (redshift-independent) distance measurements. Due to the large uncertainties present in galaxy distance measurements, individual galaxy radial peculiar velocities are poorly known. The resulting radial velocity field must therefore be smoothed over

a large scale to reduce the velocity errors. The full 3-dimensional velocity field is then inferred from the radial velocity field using the POTENT method proposed by Bertschinger & Dekel (1989), under the assumption that galaxy velocities trace the gravitational potential field of the underlying mass distribution. Finally, the divergence of this smoothed 3-dimensional velocity field yields the linear-theory prediction for the smoothed mass density field. On the other side of the density-density comparison, the real space galaxy density field is obtained from a galaxy redshift catalog, after correcting the galaxy redshifts for peculiar velocities estimated using the redshift space density field itself. The real-space galaxy density field is then smoothed on the same scale as the velocity field. After all of these steps are taken, the observed galaxy density field may be directly compared to the predicted mass density field. As shown by equation (3), the slope of this comparison yields  $\beta$ .

In practice, a non-linear generalization of equation (3) is used to determine  $\beta$  (e.g., Dekel et al. 1993; Hudson et al. 1995; Sigad et al. 1998; Dekel et al. 1999). For example, Sigad et al. (1998) measure  $\beta$  from a comparison of the IRAS 1.2-Jy galaxy density field,  $\delta_{IRAS}$ , to the mass density field derived from Mark III peculiar velocities. They predict the mass density field using the non-linear approximation

$$\delta_{POT} = -(1 + \epsilon_1)f^{-1}\vec{\nabla} \cdot \mathbf{v} + (1 + \epsilon_2)f^{-2}\Delta_2 + (1 + \epsilon_3)f^{-3}\Delta_3, \quad (4)$$

where  $\Delta_2$  and  $\Delta_3$  are second and third order terms that involve sums of double and triple products of partial derivatives of the velocity field, and the three coefficients  $\epsilon_1$ ,  $\epsilon_2$  and  $\epsilon_3$  are empirically determined from a family of CDM N-body simulations. In addition, Sigad et al. (1998) use a non-linear approximation to convert the IRAS galaxy redshift map to real space. Since equation (4) contains higher powers of  $f(\Omega_m)$ , it is not possible to measure  $\beta$  simply by fitting a line through the  $\delta_{IRAS}$  vs.  $\delta_{POT}$  relation. Sigad et al. (1998) first assume a value for  $\Omega_m$  and then fit a line through the relation to get  $b^{-1}$ . Their estimate for  $\beta$  is then equal to  $f(\Omega_m)/b$ . Since the initial choice of  $\Omega_m$  does not seem to affect the final  $\beta$  measurement, it appears that it is indeed a degenerate combination of  $\Omega_m$  and  $b$ , even in this mildly non-linear regime.

Aside from addressing non-linear effects, density-density analyses must deal with a host of problems that arise due to the imperfect nature of observational data sets. In particular, the peculiar velocity errors, when smoothed, give rise to inhomogeneous Malmquist bias, which is difficult to correct for. Moreover, density-density analyses must deal with issues such as non-uniform sampling and imperfect survey boundaries in both the galaxy redshift, and peculiar velocity data. Sparse sampling of the velocity field, for example, makes it particularly hard to smooth the velocity data in an unbiased way. Much work has been done recently to understand and control all of these problems (Dekel et al. 1999). Current density-density comparisons smooth the velocity field with a Gaussian filter of radius  $12h^{-1}\text{Mpc}$  and yield rather high values of  $\beta$  compared to other techniques (see Table 1 for a summary of current measurements). The analysis of Sigad et al. (1998) yields  $\beta_{IRAS} = 0.89 \pm 0.12$ .

We wish to focus directly on the influence of bias on density-density comparisons, and we therefore adopt a simpler approach to analyzing our numerical data sets. We assume perfect knowledge of both the real-space positions and the velocities of galaxies in our simulation volume. We then smooth the galaxy velocity field with a Gaussian filter of some radius  $R$  and compare its divergence to the galaxy density field smoothed at the same scale. We fit a line of form

$-(\vec{\nabla} \cdot \mathbf{v}) = \beta \delta_g + C$  to the density-density relation in the region  $-0.5 < \delta_g < 0.5$  in order to estimate  $\beta$ . Figures 1 and 2 show this procedure when the velocity and density fields are smoothed at  $12h^{-1}\text{Mpc}$  for the  $\Omega_m = 1.0$  and  $0.2$  models. In each panel we show the mean relation between  $-(\vec{\nabla} \cdot \mathbf{v})$  and  $\delta_g$  for a given bias prescription, along with its  $1\sigma$  scatter, and the best-fit line to this relation (we have omitted the Sigma and High- $z$  bias prescriptions because they produce results that are nearly identical to the Threshold and Power-law prescriptions, respectively). The slope  $\beta_{\text{fit}}$  of the best-fit line is indicated at the lower right corner of each panel. Also shown, for purposes of comparison, is the asymptotic large-scale value of  $\beta_\sigma(R)$ . Table 2 summarizes the results for all the biasing models (including the Sigma and High- $z$  bias models) for each of the three cosmological models.

For  $\Omega_m = 1.0$  and  $0.4$ , all the bias models, with the exception of the Sqrt-Exp and Sheet models, have best-fit estimates of  $\beta$  that are in excellent agreement with the asymptotic large-scale value  $\beta_\sigma$ , deviating not more than 4% from this value. The Sqrt-Exp model yields a best-fit value that is substantially higher than  $\beta_\sigma$ , whereas the Sheet model yields a  $\beta$  estimate that is somewhat lower than  $\beta_\sigma$ . However, the strong degree of non-linearity in the  $-(\vec{\nabla} \cdot \mathbf{v})$  vs.  $\delta_g$  relation for both of these models is striking in appearance and can probably be ruled out with existing data (e.g., Sigad et al. 1998). For  $\Omega_m = 0.2$ , the situation is slightly different. The Semi-analytic and Power-law models yield  $\beta$  estimates that underestimate  $\beta_\sigma$  by  $\sim 10\%$ , whereas the Sqrt-Exp model yields a  $\beta$  estimate that overestimates  $\beta_\sigma$  by 8%. Of course, analyses of real data sets must deal with the additional complications of non-linearity and statistical biases, but these have been addressed in the papers cited above and depend in detail on properties of the data sets themselves. Our results show that once these challenges are met, the value of  $\beta$  derived from POTENT-like analyses should be close to the asymptotic value of  $\beta_\sigma$ , for a fairly broad range of assumptions about the form of biasing.

#### 4. Velocity-Velocity Comparison

Velocity-velocity comparisons make use of equation (1) to measure  $\beta$ . Roughly speaking, the observed galaxy redshift distribution is used to predict the peculiar velocities of individual galaxies using equation (1), with  $f(\Omega_m)$  replaced by an assumed value for  $\beta$ . These velocity predictions are then compared directly to peculiar velocity measurements made using redshift-independent distance measurements. The best estimate of  $\beta$  is that for which the predicted and measured galaxy velocities show the best agreement.

Two distinct velocity-velocity methods have been used in recent measurements of  $\beta$ . The first method, described by Willick et al. (1997), requires that the galaxy distribution be converted from redshift space to real space before it is used to predict peculiar velocities. This is a slightly tricky step, since the peculiar velocities are both the final product and a required intermediate ingredient in this process. Once the galaxy positions are corrected for redshift-space distortions, the galaxy density field must be smoothed in order to suppress the effects of non-linear evolution and shot noise. Equation (1) is then used to compute the predicted velocity field from the smoothed galaxy density field, assuming a value for  $\beta$ . Finally, a maximum likelihood analysis (VELMOD) is used to find the value of  $\beta$  that produces the best match between the predicted and

observed galaxy velocities, assuming that an individual galaxy’s velocity is the sum of the linear theory prediction and an uncorrelated “thermal” velocity. In practice, there are many technical difficulties involved in this process. To compute the predicted velocity field, the galaxy density field must be integrated over all space, as shown by equation (1). Consequently, any systematic problems in the galaxy redshift data (such as empty regions) will affect the predicted velocity field everywhere. Moreover, the true velocity at any location will be affected to some extent by density features that are outside the volume sampled by a redshift survey. Willick et al. (1997) address this issue by adding to the predicted velocity field a quadrupole term that models the tidal field arising from density features external to the volume probed by the IRAS 1.2-Jy redshift survey. The current VELMOD analysis compares the velocities predicted from the galaxy density field of the IRAS 1.2-Jy redshift survey, smoothed with a Gaussian filter of radius  $3h^{-1}\text{Mpc}$ , to the peculiar velocities in the Mark III catalog and yields  $\beta_{IRAS} = 0.5 \pm 0.04$  (Willick & Strauss 1998).

The second velocity-velocity method, described by Nusser & Davis (1994) (hereafter ND94) and first implemented by Davis, Nusser & Willick (1996), compares the galaxy density field to the observed peculiar velocity field directly in redshift space. Another important difference between this method and VELMOD is that Davis et al. (1996) do not compare predicted and observed velocities of individual galaxies. Instead, they expand both the predicted velocity field that is derived from the redshift-space galaxy density field and the velocity field that is measured from redshift-independent distances into a set of orthogonal modes. They then perform a mode-by-mode comparison of the two fields and determine the value of  $\beta$  for which the best match is obtained. The ND94 method has been applied to estimate  $\beta_{IRAS}$  by combining the 1.2-Jy redshift survey with the Mark III peculiar velocity sample, yielding  $\beta_{IRAS} = 0.6 \pm 0.2$  (Davis et al. 1996), with a surface-brightness fluctuation sample, yielding  $\beta_{IRAS} = 0.42^{+0.10}_{-0.06}$  (Blakeslee et al. 1999), and with a type Ia supernova sample, yielding  $\beta_{IRAS} = 0.4 \pm 0.15$  (Riess et al. 1997). Most recently, Nusser et al. (2000) have applied this method to the Point Source Catalog redshift survey (PSCz) and the ENEAR peculiar velocity sample to obtain  $\beta_{IRAS} = 0.5 \pm 0.1$ .

In order to investigate the effects of bias on velocity-velocity measurements of  $\beta$ , we perform a simplified VELMOD-like analysis. As in the density-density comparisons, we assume perfect knowledge of both the real-space positions and velocities of galaxies in our simulation volumes. We smooth the galaxy density field with a Gaussian filter of radius  $R$  and use equation (1) to predict the velocity field. We then interpolate to galaxy positions to find predicted velocities ( $\mathbf{v}_{\text{pred}}$ ) for all the galaxies. Finally, we compare these with the true galaxy velocities ( $\mathbf{v}_{\text{true}}$ ). The slope of the best-fit line to the  $\mathbf{v}_{\text{true}}$  vs.  $\mathbf{v}_{\text{pred}}$  relation is our measurement of  $\beta$ . We do not include a constant offset term in our fit as we did for the density-density analysis, but it would make little difference to our results because the  $\mathbf{v}_{\text{true}}$  vs.  $\mathbf{v}_{\text{pred}}$  relations are very close to linear. The offset term is important in the density-density analysis because of the non-linearity of the  $\delta_{\text{true}}$  vs.  $\delta_{\text{pred}}$  relations. Figures 3 and 4 show this procedure when the galaxy density field is smoothed with a Gaussian filter of radius  $3h^{-1}\text{Mpc}$  for our  $\Omega_m = 1.0$  and 0.2 models. In each panel we show the mean relation between  $\mathbf{v}_{\text{true}}$  and  $\mathbf{v}_{\text{pred}}$  for a given bias prescription, along with its  $1\sigma$  scatter, and the best-fit line to this relation (as before, we have omitted the Sigma and High- $z$  bias prescriptions because they produce results that are nearly identical to the Threshold and Power-law prescriptions, respectively). The slope  $\beta_{\text{fit}}$  of the best-fit line is indicated at the lower right corner of each panel. Also shown, for purposes of comparison, is the asymptotic large-scale

value of  $\beta_\sigma(R)$ . Table 2 summarizes the results for all the biasing models (including the Sigma and High- $z$  bias models) for each of the three cosmological models.

For all three cosmological models, all the bias models, with the exception of the  $\Omega_m = 1.0$  Sheet model, have best-fit estimates of  $\beta$  that agree well with the asymptotic large-scale value  $\beta_\sigma$ , deviating not more than 11% from this value. The Sheet model yields a  $\beta$  estimate that is 33% lower than  $\beta_\sigma$ .

For smoothing lengths larger than  $5h^{-1}\text{Mpc}$ , we discovered a systematic error that affects  $\beta$  estimates made using the VELMOD method, even in the case where galaxies trace mass. It arises because a smoothed quantity ( $\mathbf{v}_{\text{pred}}$ ) is compared to an unsmoothed quantity ( $\mathbf{v}_{\text{true}}$ ), and the errors in the predicted velocities are thus correlated with the predicted velocities themselves. This issue is fully explored in a previous paper (Berlind, Narayanan & Weinberg 2000). The mode-by-mode method of ND94 should not be affected by this systematic error because it effectively smooths both the velocity and the density fields in the same manner. For a smoothing length of  $3h^{-1}\text{Mpc}$ , the influence on VELMOD analyses is small, at least for the cosmological models considered here.

## 5. Anisotropy Of Redshift-Space Clustering

Both density-density and velocity-velocity methods require measurements of galaxy peculiar velocities in addition to redshifts. Peculiar velocity measurements always contain large statistical and systematic uncertainties because they rely on distance-indicator relations that have substantial intrinsic scatter as well as uncertain calibrations and environmental dependencies. Moreover, these methods usually require the galaxy density field in real space and therefore rely on a conversion of the observed redshift-space galaxy density field. There is an entirely different approach to estimating  $\beta$  that does not suffer from either of these problems, though it does require very large redshift samples for effective application. It takes advantage of the fact that line-of-sight distortions in redshift space are caused by the same velocities that density-density and velocity-velocity methods must measure independently. It is possible to estimate  $\beta$  simply by analyzing these redshift-space distortions, or, more specifically, by measuring the anisotropy of the galaxy clustering in redshift space.

Kaiser (1987) showed that, in the linear regime, the redshift-space galaxy power spectrum  $[P_g^S(k, \mu)]$  is related to the real-space galaxy power spectrum  $[P_g^R(k)]$  by

$$P_g^S(k, \mu) = (1 + \beta\mu^2)^2 P_g^R(k), \quad (5)$$

where  $\mu$  is the cosine of the angle between the line-of-sight and the wave-vector  $\mathbf{k}$  of a fluctuation in the galaxy density field. This equation is derived using the plane-parallel approximation, i.e., in the case where the volume probed is distant enough that all lines of sight to it are effectively parallel. Equation (5) reveals that the redshift-space power spectrum is anisotropic. The power spectrum of fluctuations along the line-of-sight is amplified by the amount  $(1 + \beta)^2$  with respect to the power spectrum in real space, whereas the power spectrum of fluctuations perpendicular to the line-of-sight is not affected at all. The redshift-space power spectrum (5) has been shown to

reduce to a sum of monopole ( $l = 0$ ), quadrupole ( $l = 2$ ), and hexadecapole ( $l = 4$ ) terms,

$$P_g^S(k, \mu) = P_0^S(k)L_0(\mu) + P_2^S(k)L_2(\mu) + P_4^S(k)L_4(\mu), \quad (6)$$

where  $L_l(\mu)$  are Legendre polynomials. The first two moments are related to the real space galaxy power spectrum by

$$\begin{aligned} P_0^S(k) &= \left(1 + \frac{2}{3}\beta + \frac{1}{5}\beta^2\right) P_g(k), \\ P_2^S(k) &= \left(\frac{4}{3}\beta + \frac{4}{7}\beta^2\right) P_g(k) \end{aligned} \quad (7)$$

(Cole, Fisher & Weinberg 1994). Hamilton (1992) derived a similar set of relations for the multipole moments of the redshift-space galaxy correlation function. Equations (6) and (7) provide us with two different ways to measure  $\beta$  from the redshift space power spectrum  $P^S(k, \mu)$  (from now on we will drop the subscript  $g$  in the galaxy power spectrum); using  $P^S(k)/P^R(k)$ , the ratio of the angle-averaged redshift-space power spectrum (monopole) to the real-space power spectrum, or using  $P_2(k)/P_0(k)$ , the ratio of the quadrupole and monopole moments of the redshift-space power spectrum. These ratios are, in principle, measurable and in linear theory they are related to  $\beta$  by

$$\frac{P^S(k)}{P^R(k)} = 1 + \frac{2}{3}\beta + \frac{1}{5}\beta^2, \quad (8)$$

$$\frac{P_2(k)}{P_0(k)} = \frac{(\frac{4}{3}\beta + \frac{4}{7}\beta^2)}{(1 + \frac{2}{3}\beta + \frac{1}{5}\beta^2)}. \quad (9)$$

These ratios yield an estimate of  $\beta$  at each wavenumber  $k$ . However, non-linearity in the velocity and density fields produces distortions in an opposite sense to the linear theory predictions, leading to systematically lower estimates of  $\beta$  even on scales as large as  $50h^{-1}\text{Mpc}$ . Hence, it is essential to model the non-linearities accurately in order to estimate  $\beta$  using currently available redshift surveys. Cole et al. (1995) estimated  $\beta$  from  $P_2(k)/P_0(k)$  by assuming an exponential velocity distribution model, in which galaxies have uncorrelated small scale peculiar velocities drawn from an exponential distribution in addition to their linear theory velocities. Applying this method to the IRAS 1.2-Jy redshift survey, they found  $\beta_{IRAS} = 0.52 \pm 0.13$ . Fisher & Nusser (1996) modeled the non-linearity in  $P_2(k)/P_0(k)$  by using the Zel'dovich approximation (Zel'dovich 1970), thus assuming that the scale dependence in this ratio is caused by coherent, rather than random, non-linear motions. They found  $\beta_{IRAS} = 0.6 \pm 0.2$ . Finally, Hatton & Cole (1999) proposed and tested an empirical model for the non-linearity in  $P_2(k)/P_0(k)$  by examining the scale dependence of this ratio in a large number of N-body simulations spanning a broad range of cosmological parameters. This model is more general than the previous ones because it is based on fully non-linear N-body data.

Equations (8) and (9) only hold in the linear regime and the plane-parallel approximation. In order to use these relations to measure  $\beta$ , we must measure  $P^S(k, \mu)$  in volumes that are both large (so that they contain fluctuations large enough to be in the linear regime) and far away (so that all lines of sight to a single volume are approximately parallel). These constraints make

it difficult to accurately measure  $\beta$  from the redshift surveys that exist today. Ongoing surveys, such as the 2dF redshift survey and Sloan Digital Sky Survey (SDSS), will be much better suited to this purpose because they will probe very large volumes, although even then non-linearity will be important. To avoid the need for the distant observer approximation, Fisher, Scharf & Lahav (1994) measured  $\beta$  from the IRAS 1.2-Jy redshift survey by expanding the galaxy redshift-space density field into spherical harmonics and maximizing the likelihood that an assumed real-space galaxy power spectrum would yield that specific set of harmonics. The free parameters in this spherical harmonic analysis (SHA) are  $\beta$  and  $\Gamma$ , the latter determining the shape of the real-space power spectrum. Fisher et al. (1994) obtained  $\beta_{IRAS} = 0.94 \pm 0.17$ . More recently, Ballinger et al. (2000) used the SHA method to measure  $\beta_{IRAS} = 0.40 \pm 0.10$  for the PSCz, and Hamilton, Tegmark & Padmanabhan (2000) developed an optimal way to apply the SHA method to the same survey and measured  $\beta_{IRAS} = 0.41_{-0.12}^{+0.13}$ . Table 1 gives a summary of  $\beta$  measurements from redshift-space distortions in IRAS selected galaxy redshift surveys (also see Hamilton 1998 for a review of such measurements).

For our simulation analyses, we estimate  $\beta$  from the anisotropy of the redshift-space power spectrum using an approach that is similar to that of Cole et al. (1995), but somewhat simplified. We take the line-of-sight direction to be a Cartesian axis of the simulation cube, implicitly assuming that the whole simulation volume is far enough away to satisfy the distant observer approximation. We measure  $P^S(k, \mu)$  and  $P^R(k)$  using a Fast Fourier Transform (FFT), and we extract the multipole moments by fitting equation (6) to  $P^S(k, \mu)$ . We compute the average values and  $1\sigma$  uncertainties of the ratios  $P^S(k)/P^R(k)$  and  $P_2(k)/P_0(k)$  from the four independent realizations of each galaxy distribution. The points in Figures 5 and 6 represent the functions  $\beta(\lambda)$  obtained from solving for  $\beta$  in equations (8) and (9), respectively, where  $\lambda = 2\pi/k$ . These functions asymptote to a constant value only on large scales, since equations (7) only hold under the assumption of linear theory. We estimate  $\beta$  for each bias model using two methods. (1) We use the Cole et al. (1995) exponential velocity distribution model to model the non-linearity in  $P^S(k)/P^R(k)$ , and we estimate  $\beta$  by fitting this model to our measured  $P^S(k)/P^R(k)$ . We perform the fit only using modes that correspond to scales  $\lambda > 20h^{-1}\text{Mpc}$ , and the fitting parameters are  $\beta_{\text{fit}}$  and  $\sigma_v$  (the small-scale velocity dispersion). The thick lines in Figure 5 represent the resulting fits for  $\Omega_m = 1.0$ . (2) We use the Hatton & Cole (1999) empirical model to model the non-linearity in  $P_2(k)/P_0(k)$ , and we estimate  $\beta$  by fitting this model to our measured  $P_2(k)/P_0(k)$ . As before, we perform the fit only using modes that correspond to scales  $\lambda > 20h^{-1}\text{Mpc}$ , and the fitting parameters are  $\beta_{\text{fit}}$  and  $k_{\text{nl}}$  (the wavenumber that corresponds to the scale at which the ratio  $P_2(k)/P_0(k)$  is equal to zero). The thick lines in Figure 6 represent the resulting fits for  $\Omega_m = 1.0$ . The thin lines in Figures 5 and 6 show the function  $\beta_P(\lambda) = \Omega_m^{0.6}/b_P(\lambda)$ , where  $b_P(\lambda) \equiv \sqrt{P_g(k)/P_m(k)}$  at  $k = 2\pi/\lambda$ . In both figures, the best-fit estimates  $\beta_{\text{fit}}$  are indicated at the lower right corner of each panel. Also shown, for purposes of comparison, are the asymptotic large-scale values of  $\beta_\sigma(R)$ . Table 2 summarizes these values and also includes results for the Sigma and High- $z$  bias models, which are omitted from Figures 5 and 6, and for the low  $\Omega_m$  cosmological models.

For all three cosmological models and all bias models, with the exception of the  $\Omega_m = 1.0$  Sqrt-Exp and Sheet models, the best-fit estimates of  $\beta$  made using the redshift-to-real-space ratio  $P^S(k)/P^R(k)$  underestimate  $\beta_\sigma$  by 10 – 20%. This underestimate occurs even for the unbiased

(mass) models, indicating that it arises because the exponential velocity distribution model for the non-linear behaviour of  $P^S(k)/P^R(k)$  is not accurate at this level. Cole et al. (1995) reached a similar conclusion about the accuracy of this non-linear model, in a slightly different manner. The Hatton & Cole (1999) empirical model does a better job fitting the quadrupole-to-monopole ratio  $P_2(k)/P_0(k)$ . For  $\Omega_m = 1.0$ , all of the bias models, with the exception of Sqrt-Exp and Sheet, yield  $\beta$  estimates that underestimate  $\beta_\sigma$  by 3 – 8%. For low  $\Omega_m$ , all of the bias models, again with the exception of Sqrt-Exp, yield  $\beta$  estimates that agree well with  $\beta_\sigma$ .

## 6. Summary

Figures 7, 8 and 9 summarize all of our results for  $\Omega_m = 1.0, 0.4$ , and  $0.2$ , respectively. Each panel corresponds to a particular biasing prescription and shows  $\beta$  estimates, as a function of smoothing length, made using a density-density comparison (circles) and a velocity-velocity comparison (squares). Also shown, at arbitrary scales, are the  $\beta$  estimates made from the anisotropy of redshift-space clustering (triangles). Solid points represent the smoothing scales that correspond to recent observational estimates of  $\beta$ : the density-density (POTENT-like) estimate made with a  $12h^{-1}$ Mpc Gaussian smoothing (solid circle; cf. Sigad et al. 1998), the velocity-velocity (VELMOD-like) estimate made with a  $3h^{-1}$ Mpc Gaussian smoothing (solid square; cf. Willick et al. 1997), and the redshift-space anisotropy estimate made using the quadrupole-to-monopole ratio of the redshift-space power spectrum,  $P_2(k)/P_0(k)$ , marked at an arbitrary scale (solid triangle; cf. Cole et al. 1995). Also shown, for comparison, is the function  $\beta_\sigma(R)$  (solid line).

These results allow us to answer the question “what is  $\beta$ ?”. In most cases, to a fairly good approximation, the quantity  $\beta$  estimated by these methods is close to the ratio  $\Omega_m^{0.6}/b_\sigma$ , where  $b_\sigma$  is the asymptotic, large-scale value of the function  $\sigma_g(R)/\sigma_m(R)$ . This is true for all three methods and for all three cosmological models. This reassuringly simple answer is just what one might have hoped for. In our models, the bias relation in non-linear and bias factors like  $b_\sigma(R)$  and  $b_P(k)$  are scale-dependent on small scales. Nonetheless, the value of  $\beta$  has a well-defined, intuitively sensible meaning that holds for a wide range of such models. Furthermore, measurements of  $\beta$  from density-density comparisons, velocity-velocity comparisons, and analyses of the anisotropy of redshift-space clustering, should, in principle, yield consistent results.

There are some exceptions to this simple characterization. The clearest is the Sqrt-Exp bias model, which has a strongly non-linear relation between galaxy and mass density. This model exhibits the greatest scale dependence of  $b_\sigma(R)$  and  $b_P(k)$ , and different methods of estimating  $\beta$  give very different results. However, the strikingly non-linear shape of the  $-(\vec{\nabla} \cdot \mathbf{v})$  vs.  $\delta_g$  relation for this model can be ruled out by current POTENT analysis of observational data (Sigad et al. 1998), so a bias relation with such pathological effects is probably unrealistic. Another exception is the Sheet bias model. Here the different methods yield measurements of  $\beta$  that agree well with each other, but they do not match the large-scale value  $\beta_\sigma$ .

Our results imply that non-linear local bias is unlikely to account for the large discrepancies that exist between current observational estimates of  $\beta_{IRAS}$  using different techniques. We have also performed these analyses for the non-local bias model considered by NBW, where the

relation between galaxy and mass density on the  $4h^{-1}\text{Mpc}$  scale is modulated by the larger scale environment. Although the model does not have a clearly defined asymptotic value of  $\beta_\sigma$ , the different  $\beta$  estimation methods nonetheless give results that are consistent with each other. We therefore conclude that the discrepancies among current observational estimates of  $\beta$  probably arise from the interaction between the systematic errors in the observational data sets (the redshift and peculiar velocity catalogs) and the specific details of the various analysis methods. If the observational challenges can be overcome, measurements of  $\beta$  by these methods can yield a useful, physically meaningful quantity:  $\Omega_m^{0.6}$  divided by a bias factor that characterizes the ratio of rms galaxy and mass fluctuations, on large scales.

We note with great sadness the passing of Jeff Willick, who has been a leader in this field for more than a decade. We are grateful to Jeff and to Scott Gaudi and Michael Strauss for helpful input and comments. This work was supported by NSF grant AST-9802568. AAB and VKN were supported by Presidential Fellowships from the Graduate School of The Ohio State University during phases of this project.

### References

- Babul, A., Weinberg, D. H., Dekel, A. & Ostriker, J. P. 1994, ApJ, 427, 1
- Ballinger, W. E., Taylor, A. N., Heavens, A. F. & Tadros, H. 2000, to appear in the proceedings of the XXXVth Rencontres de Moriond: Energy Densities in the Universe (astro-ph/0005094)
- Benson, A. J., Cole, S., Frenk, C. S., Baugh, C. M. & Lacey, C. G. 2000, MNRAS, 311, 793
- Berlind, A. A., Narayanan, V. K., & Weinberg, D. H. 2000, ApJ, 537, 537
- Bertschinger, E., & Dekel, A. 1989, ApJ, 336, L5
- Blakeslee, J. P., Davis, M., Tonry, J. L., Dressler, A., & Ajhar, E. A. 1999, ApJ, 527, L73
- Blanton, M., Cen, R., Ostriker, J. P. & Strauss, M. A. 1999, ApJ, 522, 590
- Bromley, B. C., Warren, M. S. & Zurek, W. H. 1997, ApJ, 475, 414
- Cen, R. & Ostriker, J. P. 1992, ApJ, 393, 22
- Cen, R. & Ostriker, J. P. 1993, ApJ, 417, 415
- Cole, S., Fisher, K. B. & Weinberg, D. H. 1994, ApJ, 267, 785
- Cole, S., Fisher, K. B. & Weinberg, D. H. 1995, ApJ, 275, 515
- Cole, S., Weinberg, D. H., Frenk, C. S., & Ratra, B. 1997, MNRAS, 289, 37
- Colín, P., Klypin, A. A., Kravtsov, A. V. & Khokhlov, A. M. 1999, ApJ, 523, 32
- Davis, M., Nusser, A., & Willick, J. 1996, ApJ, 473, 22
- Dekel, A., Bertschinger, E., Yahil, A., Strauss, M. A., Davis, M., & Huchra, J. P. 1993, ApJ, 412, 1
- Dekel, A. & Lahav, O. 1999, ApJ, 520, 24
- Dekel, A., Eldar, A., Kolatt, T., Yahil, A., Willick, J. A., Faber, S. M., Courteau, S., & Burstein, D. 1999, ApJ, 522, 1
- Efstathiou, G., Bond, J. R., & White, S. D. M. 1992, MNRAS, 258, 1P
- Fisher, K. B., Scharf, C. A. & Lahav, O. 1994, MNRAS, 266, 219
- Fisher, K. B., Huchra, J. P., Strauss, M. A., Davis, M., Yahil, A & Schlegel, D 1995, ApJS, 100, 69
- Fisher, K. B. & Nusser, A. 1996, MNRAS, 279, L1
- Hamilton, A. J. S. 1992, ApJ, 385, L5
- Hamilton, A. J. S. 1998, in The Evolving Universe, ed. Hamilton, D., (Kluwer Academic, Dordrecht) p. 185 (astro-ph/9708102)

- Hamilton, A. J. S. Tegmark, M. & Padmanabhan, N. 2000, MNRAS, submitted (astro-ph/0004334)
- Hatton, S. J. & Cole, S. 1999, MNRAS, 310, 113
- Hudson, M. J., Dekel, A., Courteau, S., Faber, S. M., & Willick, J. A. 1995, MNRAS, 274, 305
- Kaiser, N. 1987 MNRAS, 227, 1
- Katz, N., Hernquist, L. & Weinberg, D. H. 1992, ApJ, 399, L109
- Katz, N., Weinberg, D. H. & Hernquist, L. 1996, ApJS, 105, 19
- Kauffmann, G., Colberg, J. M., Diaferio, A. & White, S. D. M. 1999, MNRAS, 303, 188
- Kravtsov, A. V., & Klypin, A. A. 1999, ApJ, 520, 437
- Mann, R. G., Peacock, J. A. & Heavens, A. F. 1998, MNRAS, 293, 209
- Moore, B., Ghigna, S., Governato, F., Lake, G., Quinn, T., Stadel, J. & Tozzi, P. 1999, ApJ, 524L, 19
- Narayanan, V. K., Weinberg, D. H., Branchini, E., Frenk, C. S., Maddox, S., Oliver, S., Rowan-Robinson, M. & Saunders, W. 1999, ApJ, in press, (astro-ph/9910229)
- Narayanan, V. K., Berlind, A. A. & Weinberg, D. H. 2000, ApJ, 528, 1
- Nusser, A. & Davis, M. 1994, ApJ, 421, L1
- Nusser, A., da Costa, L. N., Branchini, E., Bernardi, M., Alonso, M. V., Wegner, G., Willmer, C. N. A. & Pellegrini, P. S. 2000, MNRAS, submitted (astro-ph/0006062)
- Park, C. 1990, PhD Thesis, Princeton University
- Pearce, F. R., Jenkins, A., Frenk, C. S., Colberg, J. M., White, S. D. M., Thomas, P. A., Couchman, H. M. P., Peacock, J. A. & Efstathiou, G. (The Virgo Consortium) ApJ, 521L, 99
- Peacock, J. A. & Dodds, S. J. 1994, MNRAS, 267, 1020
- Peebles, P. J. E. 1980, The Large-Scale Structure of the Universe, (Princeton: Princeton University Press)
- Rauzy, S. & Hendry, M. A. 2000, MNRAS, 316, 612
- Riess, A. G., Davis, M., Baker, J. & Kirschner, R. P. 1997, ApJ, 488, L1
- Sigad, Y., Eldar, A., Dekel, A., Strauss, M.A., & Yahil, A. 1998, ApJ, 495, 516
- Strauss, M. A. & Willick, J. A. 1995, Physics Reports, 261, 271
- Willick, J. A., Strauss, M. A., Dekel, A., & Kolatt, T. 1997, ApJ, 486, 629
- Willick, J. A., & Strauss, M. A. 1998, ApJ, 507, 64
- White, S. D. M., Efstathiou, G. P., & Frenk, C. S. 1993, MNRAS, 262, 1023
- Zel'dovich, Y. B. 1970, A&A, 5, 84

Table 1. Current  $\beta$  measurements for IRAS selected galaxies

Data	Method	Paper	$\beta$
IRAS 1.2-Jy + Mark III	POTENT	Sigad et al. (1998)	$0.89 \pm 0.12$
	VELMOD	Willick & Strauss (1998)	$0.50 \pm 0.04$
	ND94	Davis et al. (1996)	$0.60 \pm 0.20$
	ROBUST	Rauzy & Hendry (2000)	$0.60 \pm 0.125$
IRAS 1.2-Jy + SNIa	ND94	Riess et al. (1997)	$0.40 \pm 0.15$
IRAS 1.2-Jy + SBF	ND94	Blakeslee et al. (1999)	$0.42^{+0.10}_{-0.06}$
IRAS 1.2-Jy	$P_2(k)/P_0(k)$	Cole et al. (1995)	$0.52 \pm 0.13$
	$P_2(k)/P_0(k)$	Fisher & Nusser (1996)	$0.60 \pm 0.20$
	SHA	Fisher et al. (1994)	$0.94 \pm 0.17$
	$\sigma_{\parallel}^2/\sigma_{\perp}^2$	Bromley, Warren & Zurek (1997)	$0.80^{+0.40}_{-0.30}$
IRAS QDOT	$P^S(k)/P^R(k)$	Peacock & Dodds (1994)	$1.00 \pm 0.20$
	$P_2(k)/P_0(k)$	Cole et al. (1995)	$0.54 \pm 0.30$
PSCz + ENEAR	ND94	Nusser et al. (2000)	$0.50 \pm 0.10$
PSCz	SHA	Ballinger et al. (2000)	$0.40 \pm 0.10$
	SHA	Hamilton, Tegmark & Padmanabhan (2000)	$0.41^{+0.13}_{-0.12}$

Note—We have listed only the most recent estimates for a given data set from each group.

Table 2. Estimates of  $\beta$  from the biased models, using different techniques

Model	POTENT		VELMOD	$P^S(k)/P^R(k)$	$P_2(k)/P_0(k)$
	$\beta_\sigma$	$\beta_{\text{est}}$	$\beta_{\text{est}}$	$\beta_{\text{est}}$	$\beta_{\text{est}}$
$\Omega = 1.0$					
Mass	1.00	0.92	0.94	0.80	0.93
Semi-analytic	0.61	0.61	0.56	0.54	0.57
Sqrt-Exp.	0.62	0.84	0.69	0.64	0.98
Power-law	0.60	0.60	0.57	0.52	0.55
Threshold	0.57	0.55	0.56	0.47	0.55
Sigma	0.54	0.53	0.56	0.46	0.52
Sheet	0.66	0.53	0.44	0.46	0.52
High- $z$	0.60	0.58	0.55	0.52	0.58
$\Omega = 0.4$					
Mass	0.58	0.56	0.54	0.50	0.64
Semi-analytic	0.57	0.55	0.54	0.49	0.59
Sqrt-Exp.	0.77	0.93	0.80	0.69	0.76
$\Omega = 0.2$					
Mass	0.38	0.36	0.35	0.32	0.43
Semi-analytic	0.52	0.46	0.48	0.41	0.51
Sqrt-Exp.	0.66	0.71	0.64	0.59	0.57
Power-law	0.54	0.49	0.48	0.45	0.52

Note—POTENT results are shown for a  $12h^{-1}\text{Mpc}$  Gaussian smoothing. VELMOD results are shown for a  $3h^{-1}\text{Mpc}$  Gaussian smoothing. For  $\Omega_m = 1.0$ , all uncertainties are  $\sim 0.005$ . For low  $\Omega_m$ , uncertainties are  $\sim 0.002$ , except for Sqrt-Exp models, where they are  $\sim 0.04$  for  $\Omega_m = 0.4$  and  $\sim 0.02$  for  $\Omega_m = 0.2$ .

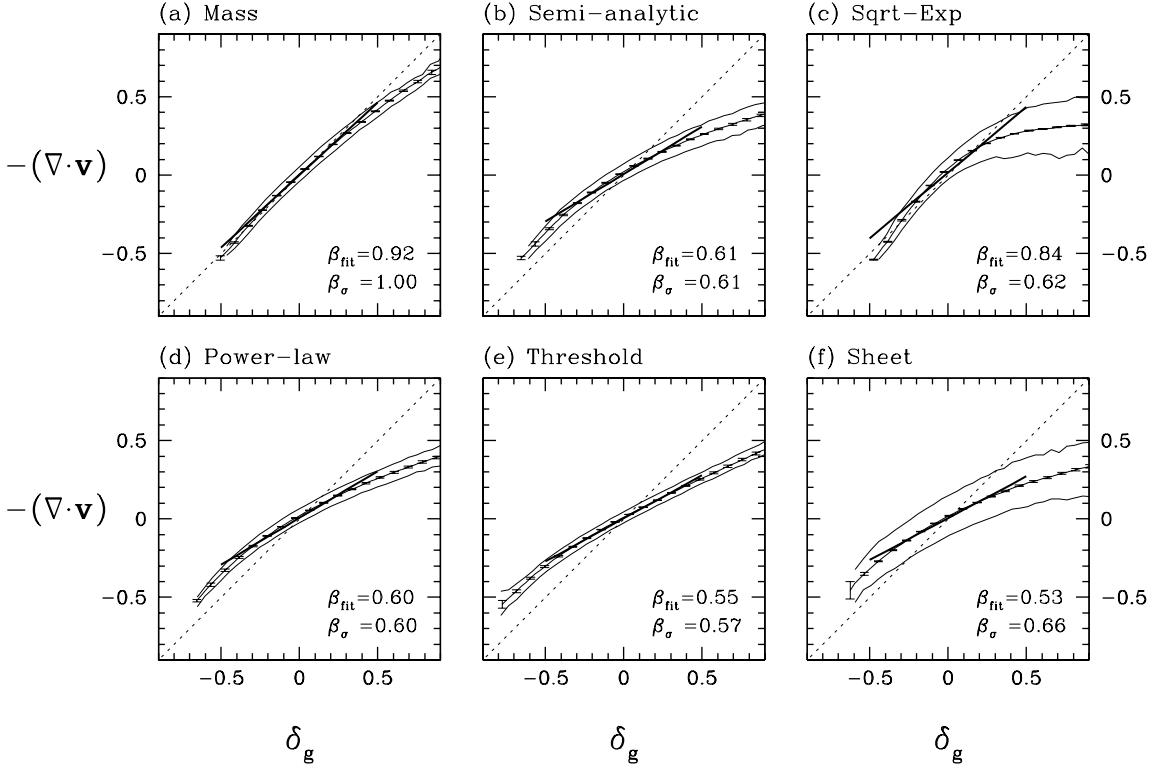


Fig. 1.— Density-density (POTENT-like)  $\beta$  estimates for our  $\Omega_m = 1.0$  cosmological model. Each panel shows the mean measured relation between  $-(\nabla \cdot \mathbf{v})$  and  $\delta_g$  (thin solid curve), when the velocity and density fields are smoothed with a Gaussian filter of radius  $12h^{-1}\text{Mpc}$ , for a particular biasing prescription (we have omitted the Sigma and High- $z$  prescriptions because they produce results that are identical to the Threshold and Power-law prescriptions, respectively). The plotted relation represents the average over four independent simulations, and error bars indicate the  $1\sigma$  dispersion in this mean relation. The outer two thin solid curves represent the locus of points that, for each bin in  $\delta_g$ , enclose 80% of the points in that bin. Also shown is the best-fit line to the  $-(\nabla \cdot \mathbf{v})$  vs.  $\delta_g$  relation (thick solid line). The slope of this line, denoted by  $\beta_{\text{fit}}$ , is listed in the lower right corner of each panel. Also listed for comparison is the asymptotic, large-scale value of  $\beta_\sigma(R)$ .

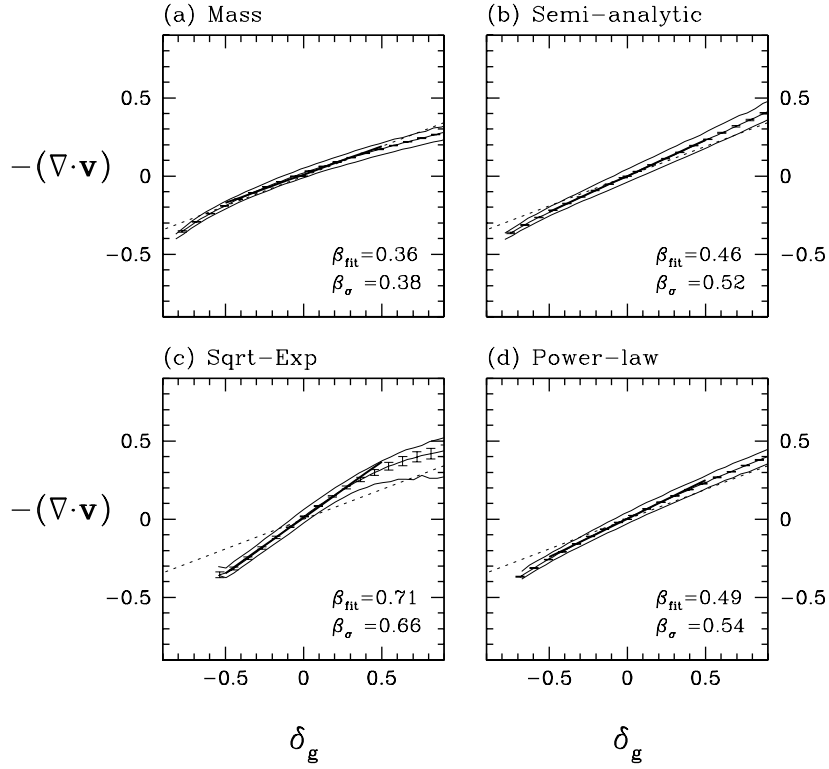


Fig. 2.— Density-density (POTENT-like)  $\beta$  estimates for our  $\Omega_m = 0.2$  cosmological model. Refer to Fig. 1 for a complete description of the components of this figure.

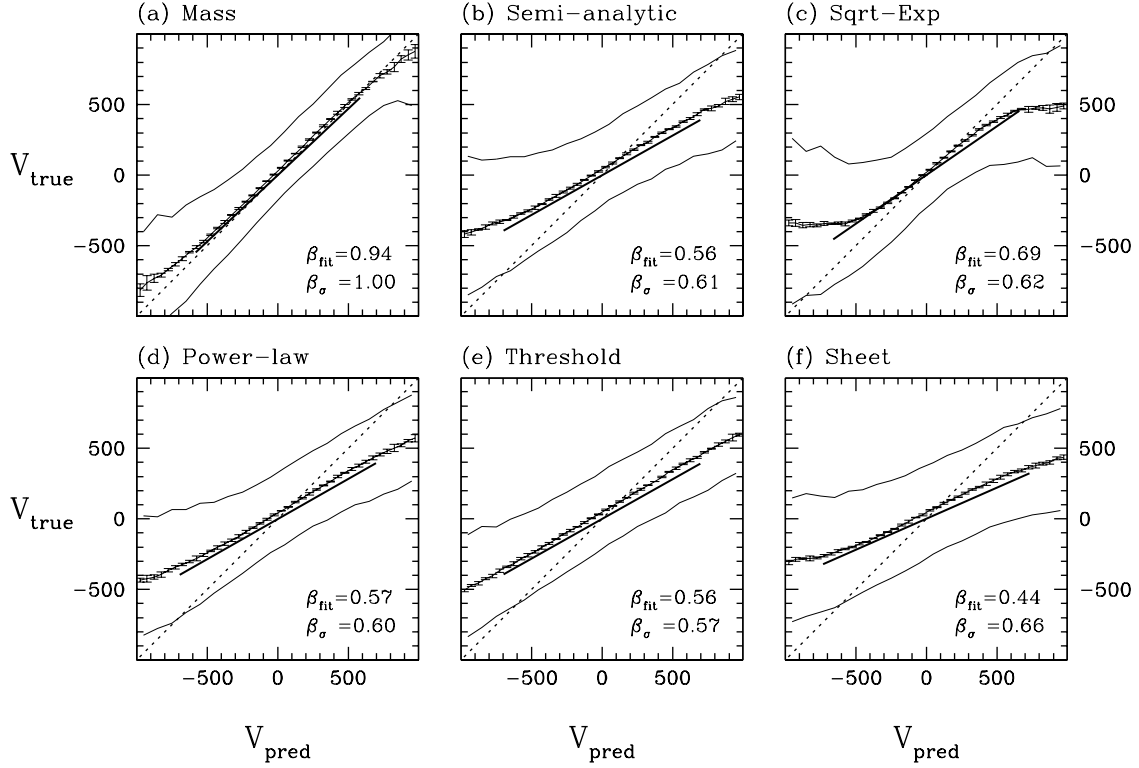


Fig. 3.— Velocity-velocity (VELMOD-like)  $\beta$  estimates for our  $\Omega_m = 1.0$  cosmological model. Each panel shows the mean measured relation between  $\mathbf{v}_{\text{true}}$  and  $\mathbf{v}_{\text{pred}}$  (thin solid curve), when the predicted velocities are computed from the galaxy density field smoothed with a Gaussian filter of radius  $3h^{-1}\text{Mpc}$ , for a particular biasing prescription (we have omitted the Sigma and High- $z$  prescriptions because they produce results that are identical to the Threshold and Power-law prescriptions, respectively). The plotted relation represents the average over four independent simulations, and error bars indicate the  $1\sigma$  dispersion in this mean relation. The outer two thin solid curves represent the locus of points that, for each value of  $\mathbf{v}_{\text{pred}}$ , enclose 80% of the galaxies. Also shown is the best-fit line to the  $\mathbf{v}_{\text{true}}$  vs.  $\mathbf{v}_{\text{pred}}$  relation (thick solid line). The slope of this line, denoted by  $\beta_{\text{fit}}$ , is listed in the lower right corner of each panel. Also listed for comparison is the asymptotic, large-scale value of  $\beta_{\sigma}(R)$ .

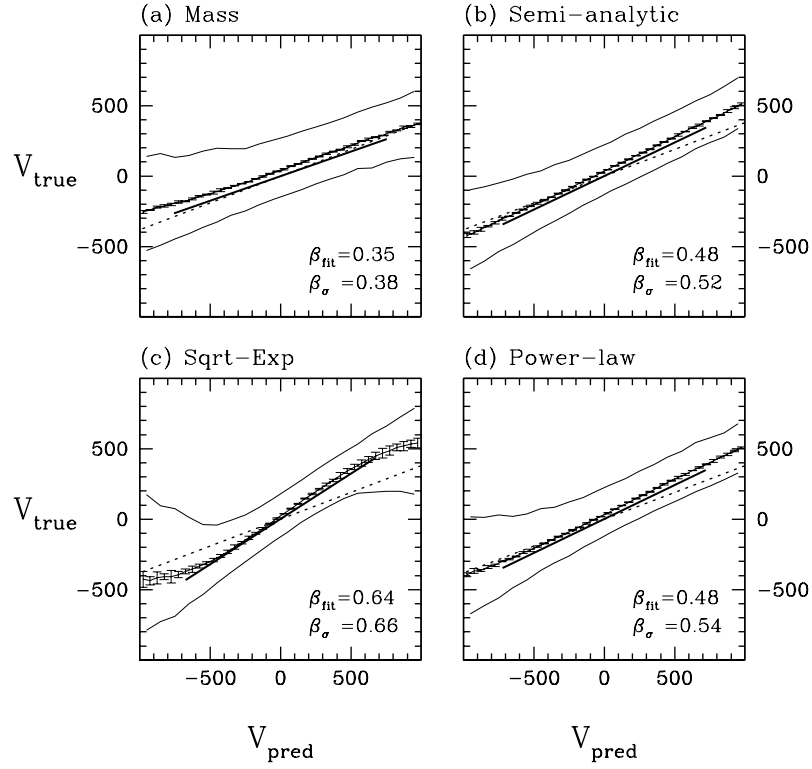


Fig. 4.— Velocity-velocity (VELMOD-like)  $\beta$  estimates for our  $\Omega_m = 0.2$  cosmological model. Refer to Fig. 3 for a complete description of the components of this figure.

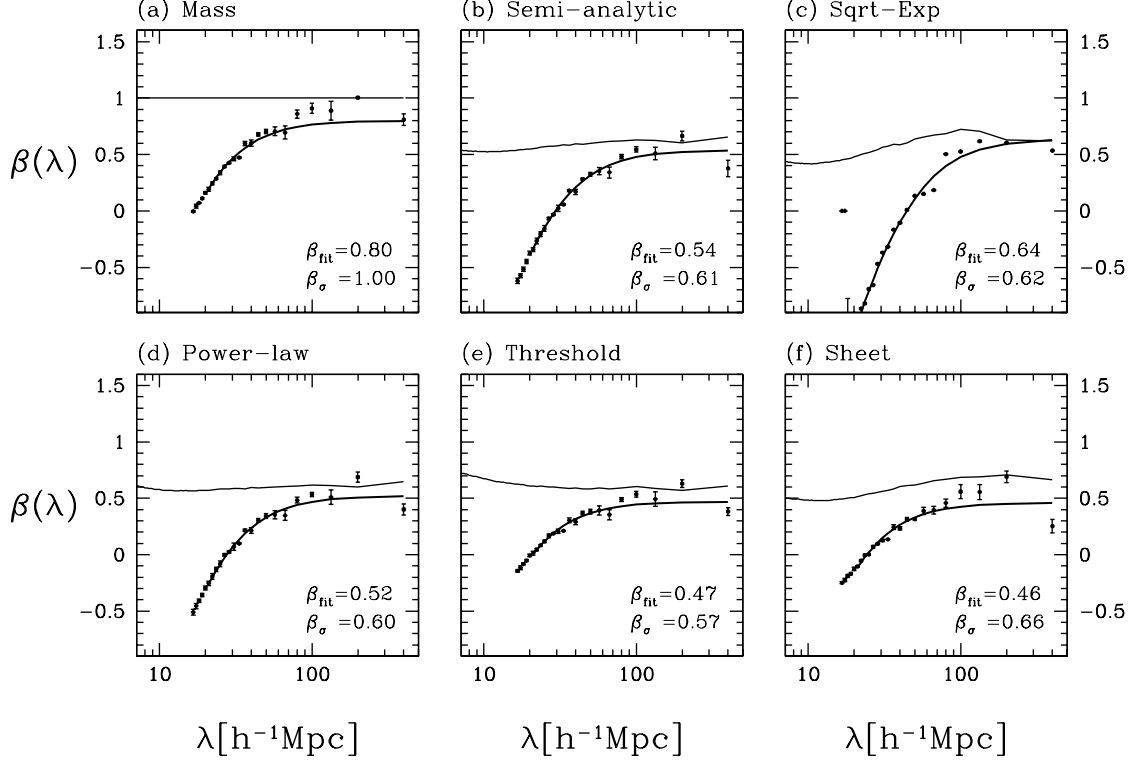


Fig. 5.— Estimates of  $\beta$  from  $P^S(k)/P^R(k)$ , the ratio of the redshift- and real-space power spectra, for our  $\Omega_m = 1.0$  cosmological model. Each panel shows an estimate of  $\beta$  for a particular biasing prescription (we have omitted the Sigma and High- $z$  prescriptions because they produce results that are identical to the Threshold and Power-law prescriptions, respectively). The points show  $\beta(\lambda)$  as estimated from  $P^S(k)/P^R(k)$  using linear theory and the plane-parallel approximation (eq. 8). The  $1\sigma$  errors in the mean  $\beta(\lambda)$  are computed using the dispersion among four independent simulations, divided by  $\sqrt{3}$ . The thin line represents the function  $\beta_P(\lambda) = \Omega_m^{0.6}/b_P(\lambda)$ , where  $b_P(\lambda)$  is the bias function, defined as  $b_P(k) = \sqrt{P_g(k)/P_m(k)}$ , where  $P_g(k)$  and  $P_m(k)$  are the power spectra of the galaxy and mass distributions, respectively. The thick line represents a fit of the exponential velocity distribution model to  $\beta(\lambda)$ . The fit yields a global estimate of  $\beta_{\text{fit}}$  which is listed at the bottom right corner of each panel. Also listed for comparison is the asymptotic, large-scale value of  $\beta_{\sigma}(R)$ .

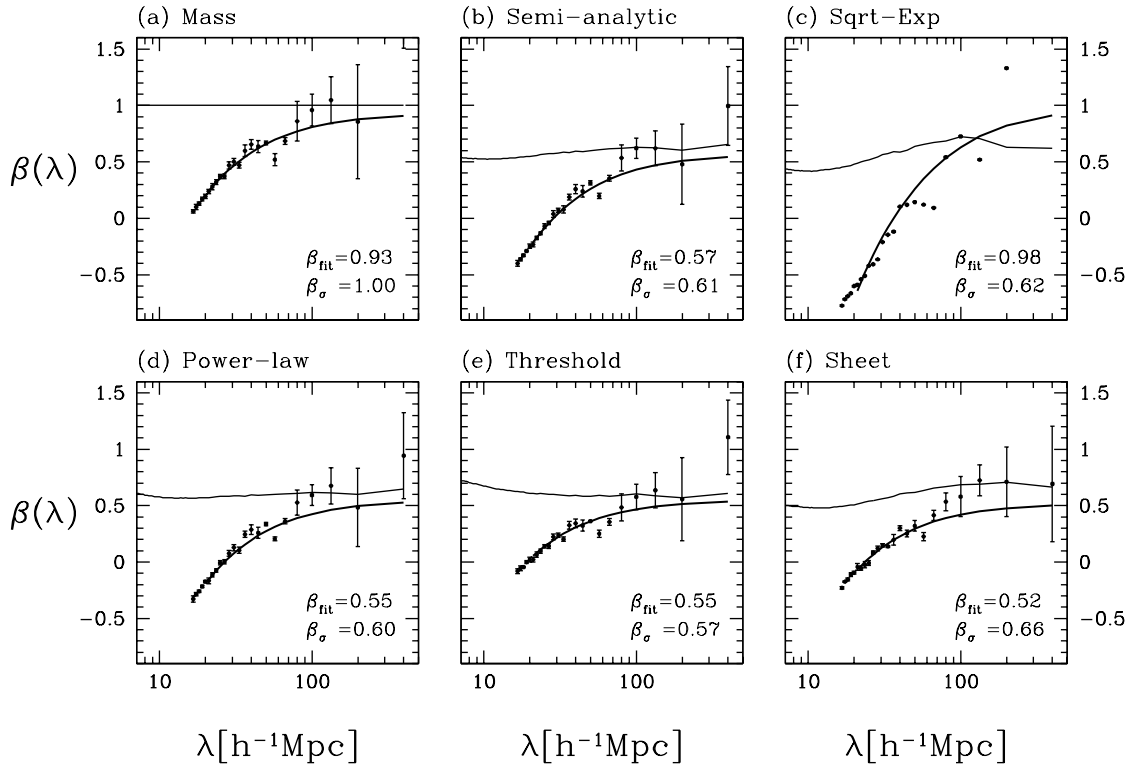


Fig. 6.— Like Fig. 5, except that  $\beta(\lambda)$  is estimated via equation (9) from  $P_2(k)/P_0(k)$ , the quadrupole-to-monopole ratio of the redshift-space power spectrum, and thick lines represent the fit of the Hatton & Cole (1999) non-linear model to  $\beta(\lambda)$ .

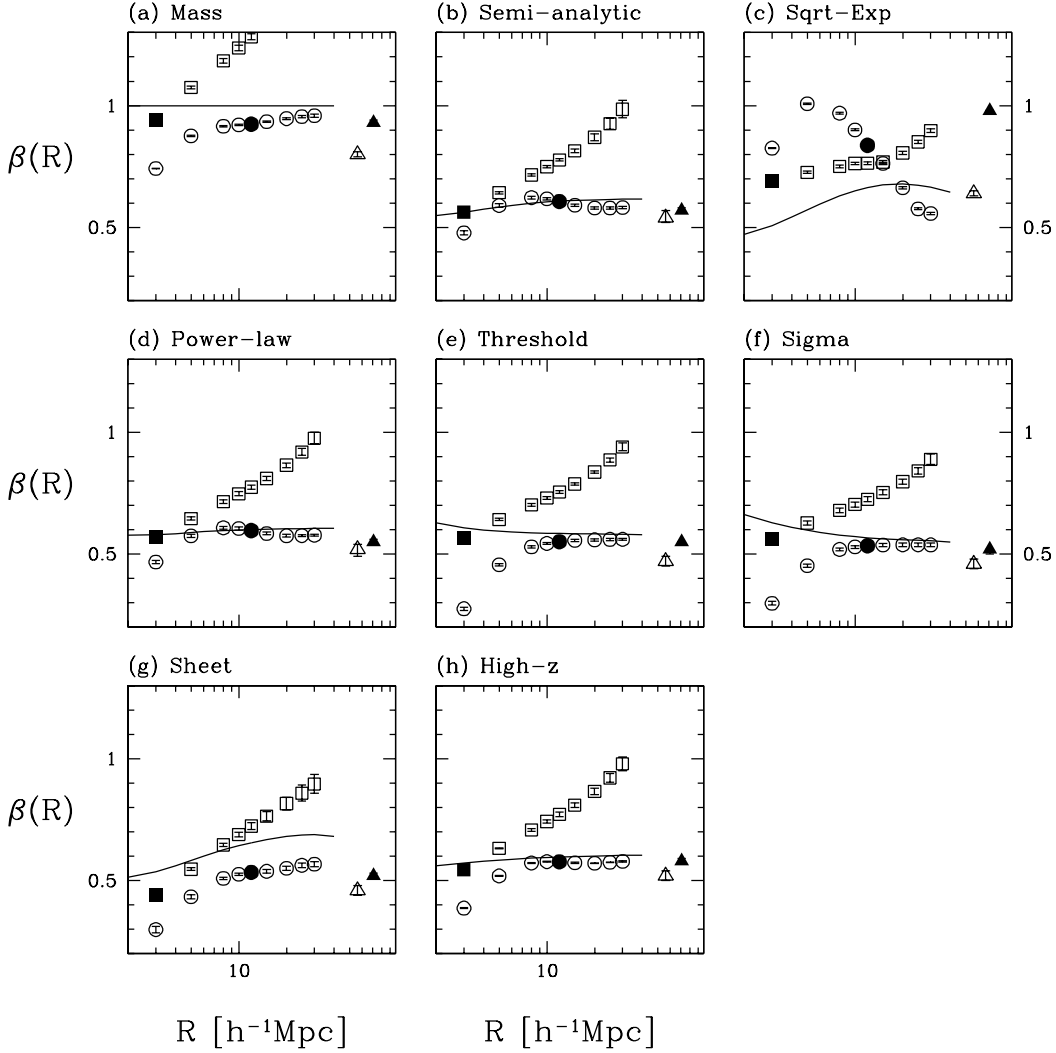


Fig. 7.— Comparison of  $\beta$  estimates from different methods, as a function of scale, for our  $\Omega_m = 1.0$  cosmological model. Each panel shows  $\beta(R)$  for a particular biasing prescription. The solid line represents the function  $\beta_\sigma(R) = \Omega_m^{0.6}/b_\sigma(R)$ , with  $b_\sigma(R) = \sigma_g(R)/\sigma_m(R)$  for a Gaussian filter of radius  $R$ . Circles represent density-density (POTENT-like)  $\beta$  estimates, derived by fitting a line to the measured relation between  $-(\nabla \cdot \mathbf{v})$  and  $\delta_g$  when the velocity and density fields are smoothed with a Gaussian filter of radius  $R$  (see Fig. 1). The  $\beta$  estimate at a  $12h^{-1}\text{Mpc}$  smoothing radius, which corresponds to current POTENT measurements, is highlighted as a solid circle. Squares represent velocity-velocity (VELMOD-like)  $\beta$  estimates, derived by fitting a line to the measured relation between  $\mathbf{v}_{\text{true}}$  and  $\mathbf{v}_{\text{pred}}$  when the predicted velocities  $\mathbf{v}_{\text{pred}}$  are estimated from the galaxy density field smoothed with a Gaussian filter of radius  $R$  (see Fig. 3). The  $\beta$  estimate at a  $3h^{-1}\text{Mpc}$  smoothing radius, which corresponds to current VELMOD measurements, is highlighted as a solid square. Triangles show estimates of  $\beta$  derived from the anisotropy of the redshift-space power spectrum. These estimates are not scale-dependent and are marked at arbitrary values of  $R$ . The open triangle shows the estimate of  $\beta$  derived from fitting the exponential velocity distribution model to  $P^S(k)/P^R(k)$  (see Fig. 5). The solid triangle shows the estimate of  $\beta$  derived from fitting the Hatton & Cole (1999) non-linear model to  $P_2(k)/P_0(k)$  (see Fig. 6). In all cases, each point represents the average over four independent simulations, and the errorbar represents the  $1\sigma$  uncertainty in the mean.

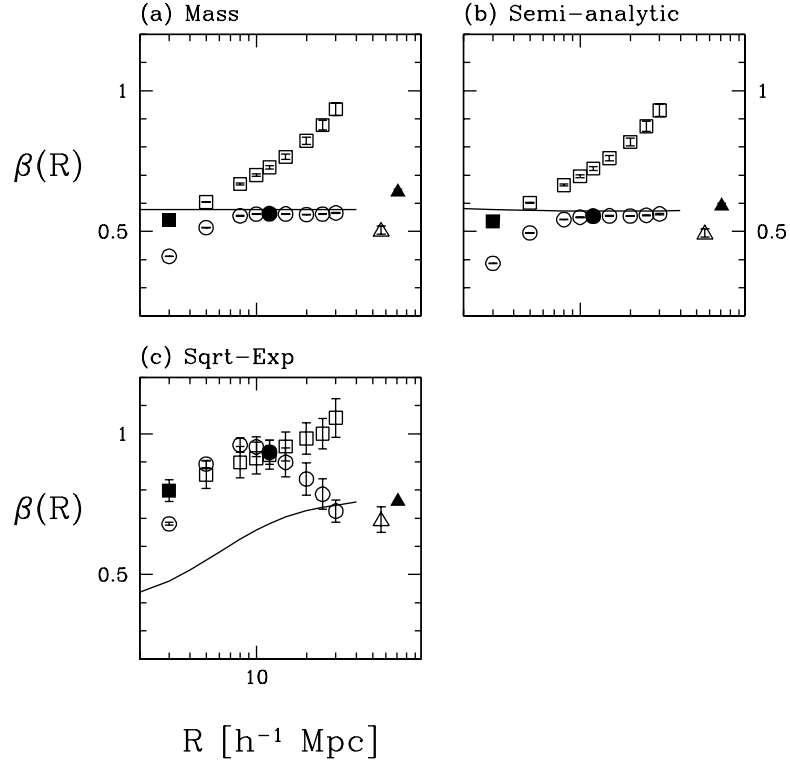


Fig. 8.— Comparison of  $\beta$  estimates from different methods, as a function of scale, for our  $\Omega_m = 0.4$  cosmological model. Each panel shows  $\beta(R)$  for a particular biasing prescription. Refer to Fig. 7 for a complete description of the components of this figure.

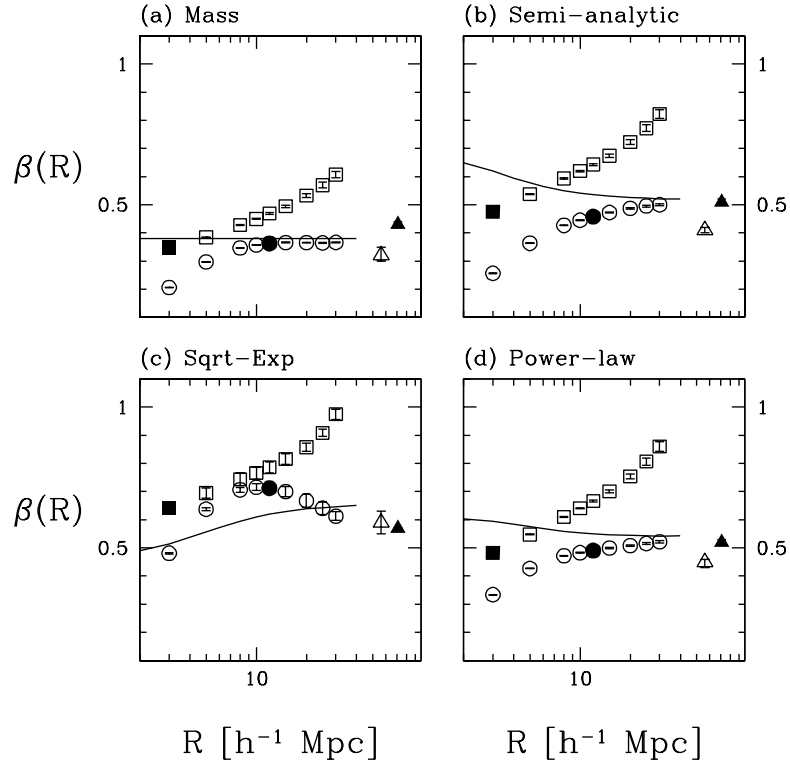


Fig. 9.— Comparison of  $\beta$  estimates from different methods, as a function of scale, for our  $\Omega_m = 0.2$  cosmological model. Each panel shows  $\beta(R)$  for a particular biasing prescription. Refer to Fig. 7 for a complete description of the components of this figure.